

NJC

Accepted Manuscript



This is an *Accepted Manuscript*, which has been through the Royal Society of Chemistry peer review process and has been accepted for publication.

Accepted Manuscripts are published online shortly after acceptance, before technical editing, formatting and proof reading. Using this free service, authors can make their results available to the community, in citable form, before we publish the edited article. We will replace this *Accepted Manuscript* with the edited and formatted *Advance Article* as soon as it is available.

You can find more information about *Accepted Manuscripts* in the [Information for Authors](#).

Please note that technical editing may introduce minor changes to the text and/or graphics, which may alter content. The journal's standard [Terms & Conditions](#) and the [Ethical guidelines](#) still apply. In no event shall the Royal Society of Chemistry be held responsible for any errors or omissions in this *Accepted Manuscript* or any consequences arising from the use of any information it contains.

Metal cluster-deposited graphene as adsorptive materials for *m*-xylene

Anchalee Junkaew,^a Chompoonut Rungnim,^a Manaschai Kunaseth,^a Raymundo Arróyave,^b
Vinich Promarak,^c Nawe Kungwan,^d and Supawadee Namuangruk^{a,*}

^a NANOTEC, National Science and Technology Development Agency (NSTDA), 111 Thailand
Science Park, Phahonyothin, Khlong Nueng, Khlong Luang, Pathum Thani 12120, Thailand

^b Department of Materials Science and Engineering, Texas A&M University, College Station, TX
77843-3003, USA

^c Vidyasirimedhi Institute of Science and Technology, Wang Chan, Rayong 21210, Thailand

^d Department of Chemistry, Faculty of Science, Chiang Mai University, Chiang Mai 50200,
Thailand

Abstract

Tetramer clusters of platinum (Pt), palladium (Pd), gold (Au) and silver (Ag) deposited on pristine and defective graphenes were studied as potential adsorptive materials for *m*-xylene using density functional theory (DFT) calculations including van der Waals contributions to the Hamiltonian. Structural, energetic and electronic (i.e. *d*-band center, partial density of state and explicit charge) properties have been investigated for understanding the *m*-xylene adsorption process. The *m*-xylene adsorption capability in these materials has been compared. The calculation results revealed that Pt₄- and Pd₄-DG adsorb *m*-xylene via chemisorption process, while Au₄- and Ag₄-DG adsorb *m*-xylene via physisorption. These insights are valuable for applying and developing carbon-based materials in volatile organic compounds (VOC) removal applications, since physisorption-driven materials are suitable as sorbents while their chemisorption

counterparts are suitable as catalysts in an oxidation reaction. Those properties in turn can be tuned by modulating the metal adsorption on the carbon-based materials.

Keywords: VOC removal, *m*-Xylene, Metal-deposited graphene, Adsorbent, DFT

* E-mail: supawadee@nanotec.or.th (S.N.),

Fax: +66(0)2564 6985; Tel. +66(0)2564 6705

1. Introduction

Volatile organic compounds (VOCs) are toxic and odorous¹⁻³ and photochemical reactions between VOCs and other pollutants originate toxic products and photochemical smog. They are released from various sources including automobiles, refineries, petrochemical units, chemical plants, *etc.*^{2, 4, 5} Many abatement techniques such as combustion, adsorption, bio-filtration, bio degradation and catalytic oxidation have been used for removing VOCs. Activated carbons (ACs), zeolites, metal organic frameworks (MOFs) and metal-doped metal oxides have been extensively explored in this field of research.^{4, 6-10} In industry, ACs have been widely used as adsorbents for removing large amount of VOCs in the primary step, since they are relatively inexpensive, large surface area, a variety of pore sizes and reusability.^{11, 12} However, some amounts of VOCs are still leaked. Nowadays, improvement of the VOC abatement technology is still challenging, particularly at trace amounts of VOCs.

Surface modification and deposition of noble and transition metals have been proposed for enhancing the VOC treatment efficiency in ACs.¹³⁻¹⁶ From the past, the adsorption of aromatic compounds on surfaces of noble- and transition metals have been broadly explored.¹⁷⁻¹⁹ Also, the

adsorption of aromatic on metal clusters have been determined by theoretical works.^{20, 21} The interactions between aromatic compounds and those metals depend on the nature of the metal. Although many metals exhibit good adsorptive and catalytic properties, they are usually expensive and their wide deployment may not be cost effective. In metal-carbon composites, good adsorptive and catalytic properties are attained by metals, while large surface areas and relatively competitive costs are provided by carbon supports.

Among VOCs, xylene is one of the more hazardous aromatic substances found in polluted air. Three isomers of xylene (*i.e.* *m*-xylene, *p*-xylene and *o*-xylene) have different positions of two methyl groups. Xylene treatments in metal-deposited carbon materials have been experimentally investigated previously.^{15, 16, 22, 23} For example, Shaoyong *et al.*²³ investigated the Pd/AC as adsorption-catalysis system for removing *o*-xylene at low concentrations. First, *o*-xylene molecules were adsorbed on the Pd/AC, and then saturated *o*-xylene-adsorbed Pd/AC were completely oxidized by feeding O₂. The experiment indicated that the *o*-xylene adsorption on the substrate is the rate-determining step. In the 5% Pd on AC, *o*-xylene were completely oxidized at 140 °C. Reduction of cost/fuel consumption and increase in energy efficiency can result from combining the adsorption and oxidation steps into one system. In another work, a regenerated Pt/AC was used for the heterogeneous adsorption and catalytic oxidation of benzene, toluene and *o*-xylene.¹⁵ That study suggested that increasing the adsorption affinity leads to lowering of oxidation temperature. This aspect suggests that the catalytic activity of the catalyst correlates to its adsorption capability.

In this work, four metal tetramers (Pt₄, Pd₄, Au₄ and Ag₄) on pristine graphene (PG) and defective graphene (DG) were selected as substrates. Our calculations were performed by using a Density Functional Theory (DFT) method including van der Waal (vdW) interactions. The

optimized structures of those metal-DG complexes were used to adsorb *m*-xylene as DG is thought to be a superior substrate than PG. The adsorption processes of *m*-xylene on the studied systems were investigated by the characterizations of structures, adsorption energy, finite charge transfer and density of states (DOS). The objective of this theoretical work is to understand the factors promoting the interactions and selectivity of *m*-xylene on those substrates. The information will likely be useful for applying these substrates in suitable techniques such as using as the adsorptive materials for the sorption-desorption techniques or promoting them to further catalytic oxidation processes.

2. Method

The generalized gradient approximation (GGA) refined by Perdew, Burke and Ernzerhof (PBE)²⁴ with projector-augmented wave (PAW)²⁵ method implemented in the Vienna *ab initio* Simulation Package (VASP)^{26, 27} was used in this work. Tkatchenko and Scheffler method with the self-consistent screening (TS+SCS)²⁸ was applied for including the vdW correction. The energy cutoff of 480 eV and the energy convergence of 1×10^{-6} eV/cell were applied in all cases. Spin-unrestricted calculation and Gaussian smearing with $\sigma = 0.1$ were used. Monkhorst-Pack was used in these calculations. Both PG and DG models were deposited with small metal clusters (tetramers). Isolated Pt, Pd, Au, Ag tetramers were placed in a vacuum box of $15.00 \text{ \AA} \times 15.00 \text{ \AA} \times 15.00 \text{ \AA}$. In slab system, metal-deposited graphene (5x5) was in simulation cell size of $12.31 \text{ \AA} \times 12.32 \text{ \AA} \times 15.00 \text{ \AA}$; the 15 \AA in the c-direction is enough to avoid the interaction between their replicas. The k-points grid of $5 \times 5 \times 1$ was used for those slab calculations.

The adsorption energy (E_{ad}) can be derived using:

$$E_{ad} = E_{X-substrate}^{complex} - E_{substrate}^{isolate} - E_X^{isolate} \quad (1)$$

where $E_{X-substrate}^{complex}$ is the total energy of an adsorbate-substrate complex. $E_{substrate}^{isolate}$ and $E_X^{isolate}$ are the total energies of a bare substrate and an isolated adsorbate (X), respectively. In the deposition of metal on graphene sheet, X represents metal tetramers and *substrate* represent PG or DG. In the *m*-xylene adsorption part, the E_{ad} of *m*-xylene on the metal-deposited DG was calculated by applying Eq. (1). The substrate and X in the equation are the metal-deposited DG and *m*-xylene, respectively.

3. Results

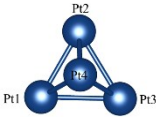
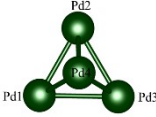
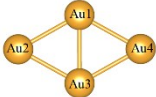
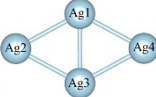
3.1 Metal-deposited graphene

First, the adsorption of Pt, Pd, Ag and Au tetramers on PG and DG has been investigated in this part. The single vacancy graphene is used as the substrate in the DG case. The calculated E_{ad} values of four metal tetramers on graphene sheets are examined in this section.

3.1.1 Properties of isolated metal clusters

In order to obtain E_{ad} of the metal-deposited graphene, the isolated metal clusters were optimized and calculated energies were used as the reference values. The most stable structures of four tetramers and their cohesive energies per atom (E_{coh}) are given in **Table 1**. The E_{coh} is calculated from $E_{coh} = (E_{cluster} - 4E_{atom})/4$, where $E_{cluster}$ and E_{atom} are the total energy of the metal cluster and its atomic energy in the gas phase, respectively. The value “4” is the number of atoms in the cluster. The calculated E_{coh} values agree well with the references as presented in **Table 1**.

Table 1: The calculated cohesive energies (E_{coh}) in eV/atom and bond length (d) in Å of the most stable structures of Pt_4 , Pd_4 , Ag_4 and Au_4 in gas phase

Metal cluster	Bond length, d (Å) of i and j	E_{coh} (eV/atom)	
		This work	Ref.
Distorted tetrahedral Pt_4	$\text{Pt}^1\text{-Pt}^2 = 2.502$  $\text{Pt}^3\text{-Pt}^4 = 2.571$ $\text{Pt}^1\text{-Pt}^3 = \text{Pt}^2\text{-Pt}^3 = \text{Pt}^1\text{-Pt}^4 =$ $\text{Pt}^2\text{-Pt}^4 = 2.604$	-2.72	-2.68 ^a , -2.4 ^b
Distorted tetrahedral Pd_4	$\text{Pd}^1\text{-Pd}^2 = \text{Pd}^3\text{-Pd}^4 = 2.549$  $\text{Pd}^1\text{-Pd}^3 = \text{Pd}^2\text{-Pd}^3 = \text{Pd}^1\text{-Pd}^4 =$ $\text{Pd}^2\text{-Pd}^4 = 2.617$	-1.69	-1.65 ^c
Rhombus Au_4	$\text{Au}^1\text{-Au}^3 = 2.618$  $\text{Au}^1\text{-Au}^2 = \text{Au}^1\text{-Au}^4 =$ $\text{Au}^2\text{-Au}^3 = \text{Au}^3\text{-Au}^4 = 2.678$ (D_{2h})	-1.55	-1.74 ^d , -1.6 ^e
Rhombus Ag_4	$\text{Ag}^1\text{-Ag}^3 = 2.605$  $\text{Ag}^1\text{-Ag}^2 = \text{Ag}^1\text{-Ag}^4 =$ $\text{Ag}^2\text{-Ag}^3 = \text{Ag}^3\text{-Ag}^4 = 2.735$ (D_{2h})	-1.16	-1.105 ^c

a²⁹, b³⁰, c³¹, d³², e³³

From the structural optimizations, the four metals can be divided into two groups according to their group series and stable geometries. In the *5d* series, the Pt₄ and Pd₄ clusters are stable in the distorted tetrahedral shape. The distorted tetrahedral structure of Pt₄ have bond lengths of around ~2.50 to 2.60 Å. This result agrees with structures reported by Xiao *et al.*²⁹ and Lin *et al.*³⁰ The high symmetry tetrahedron (C_{2v}) is distorted due to the Jahn—Teller effect. The same analysis can be applied to the Pd₄ case. The bond lengths in Pd₄ are in the range of 2.55 to 2.62 Å. In contrast, the *4d* metal clusters, the Au and Ag tetramers, prefer the rhombohedral shape as shown in **Table 1**. The short diagonal and side arms of the rhombus Au₄ are ~2.62 and ~2.68 Å, respectively. In the rhombus Ag₄, the short diagonal and side arm lengths are about 2.60 and 2.74 Å, respectively. Structural parameters are in good agreement with values from the literature.³⁴

3.1.2 Stability of metal clusters on pristine and defective graphenes

The stability of four metal tetramers-deposited on graphene was investigated by calculating E_{ad} . More negative of E_{ad} implies higher stability or stronger attraction of the metal tetramer on PG or DG. According to many possibilities of cluster arrangement on PG and DG, possible configurations found after optimization are revealed in **Figures S1-S4**. As a result, the E_{ad} values of the most stable configurations of four metal tetramers adsorbed on graphene sheets are demonstrated in **Figure 1**. In both PG and DG substrates, Pt and Pd tetramers are bound with the substrates much stronger than Au and Ag tetramers. The order of calculated E_{ad} values is Pt₄-DG (-8.30 eV) < Pd₄-DG (-6.16 eV) < Au₄-DG (-4.07 eV) < Ag₄-DG (-2.76 eV) < Pt₄-PG (-2.47 eV) < Pd₄-PG (-1.49 eV) < Au₄-PG (-1.39 eV) < Ag₄-PG (-1.06 eV). The bond lengths are measured and labeled in the **Figure 2**.

Both Pt₄ and Pd₄ are stabilized in the distorted tetrahedral geometry on both PG and DG substrates. In these two clusters, one edge of the cluster is attached to PG, where two metal atoms are bound to the bridge sites of C-C bonds of graphene (see **Figures 2a** and **2c**). On DG substrate, one metal atom is attached at the vacancy site of DG, two metal atoms are above two bridge sites as expressed in **Figures 2b** and **2d**.

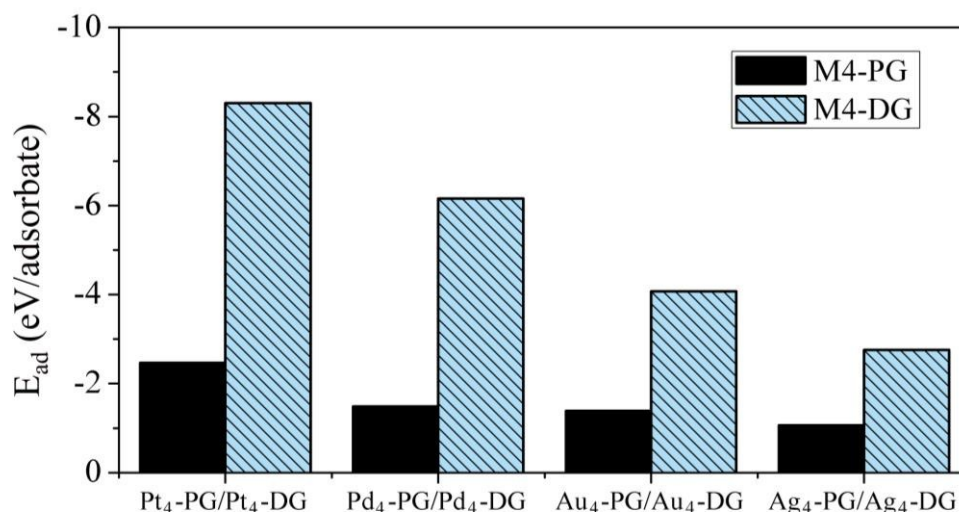


Figure 1: Comparison of the calculated E_{ad} values of the most stable structure of each metal tetramer on substrate.

Contrarily, Au₄ transforms to the Y-shape-liked structure instead of the rhombohedral shape found in the isolated Au₄ phase. The Au₄-PG and the Au₄-DG structures are illustrated in **Figures 2e** and **2f**, respectively. On both PG and DG sheets (see **Figures 2g** and **2h**), the rhombohedral Ag₄ is the preferred configuration, similarly to the structure found in the isolated Ag₄. In Ag₄-PG, the Ag₄ cluster lies parallel to the perfect graphene plane. The Ag-Ag bond lengths are varying between 2.61 to 2.74 Å which are almost retained as the values of the isolated Ag₄ in gas phase. Weak interaction between Ag₄ and PG is indicated by the average distance of ~3.4 Å. Also, this

weak interaction between Ag and C atoms has been observed in literature.³⁵ The interaction between Ag-Ag atoms is stronger than the Ag-C interaction. One Ag atom is anchored at the vacancy site of DG and Ag₄ plane is tilted about 60° with respect to the DG plane.

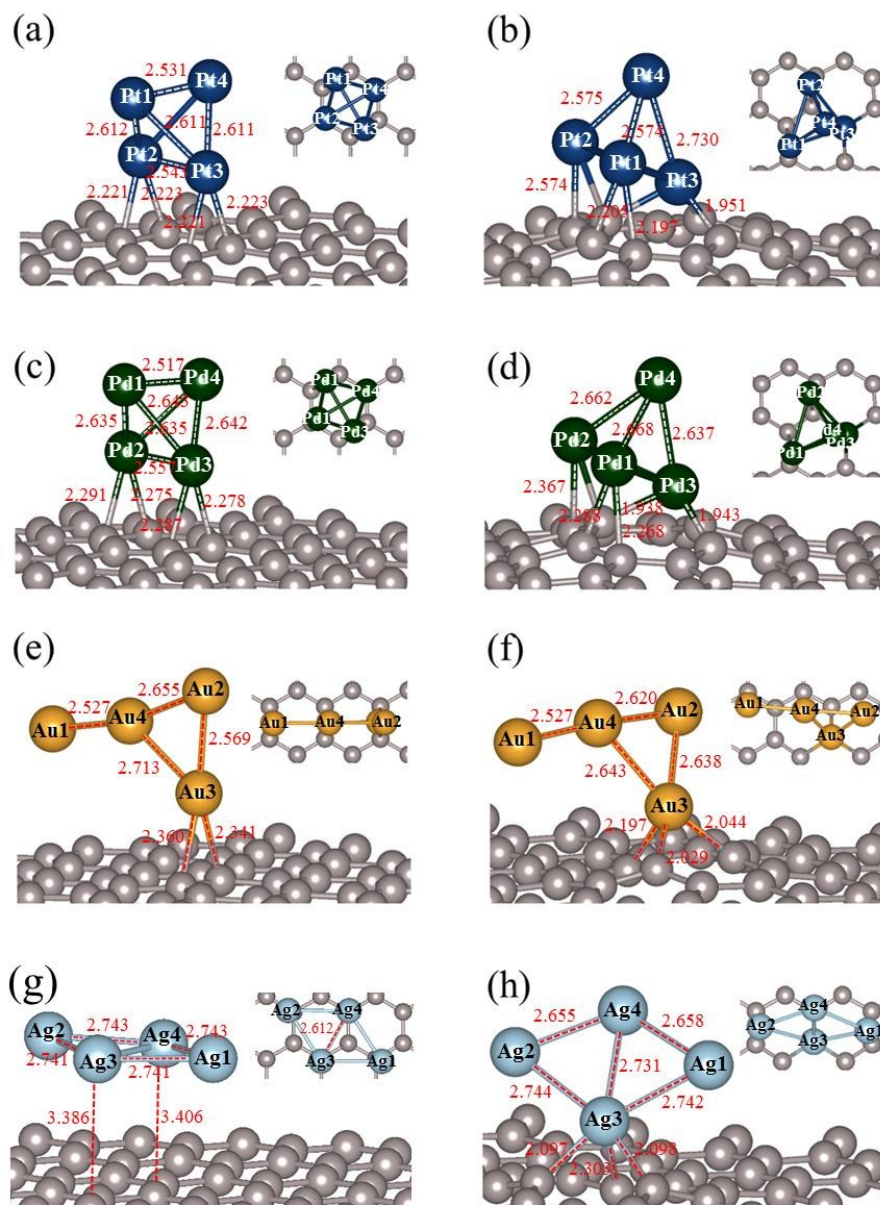


Figure 2. Metal cluster-deposited graphene (a) Pt₄-PG, (b) Pt₄-DG, (c) Pd₄-PG, (d) Pd₄-DG, (e) Au₄-PG, (f) Au₄-DG, (g) Ag₄-PG and (h) Ag₄-DG. Bond lengths are labeled in Å. Blue, green, yellow, light blue and grey balls represent Pt, Pd, Au, Ag and C atoms, respectively.

Based on energetic arguments, the results indicate that the defective site of DG poses a strong binding trap of the metal deposition. Metals bind at the vacancy site of DG much stronger than binding on a perfect sheet of PG. This may help in the suppression of metal aggregation on DG sheet compared to PG. The large adsorption energies of Pt₄ and Pd₄ on DG predict that the formed metal-DG composite sorbents would be stable at high temperature and the sorbents may be regenerated after use. According to their high adsorption stability, four tetramer-deposited DG systems were chosen as the substrates for adsorbing *m*-xylene in the next section.

3.2 Xylene adsorption on metal-deposited defective graphene

3.2.1 Xylene adsorption energy

In this part, four metal-deposited DGs were used as substrates for adsorbing *m*-xylene. From the calculation, the E_{ad} values of *m*-xylene on PG and DG are -0.98 and -0.96 eV, respectively. The E_{ad} values of *m*-xylene on Pt₄-DG, Pd₄-DG, Au₄-DG and Ag₄-DG substrates are compared in **Figure 3a**, where E_{ad} of *m*-xylene on PG is used as a reference (a red dash line). As a result, *m*-xylene has stronger interaction toward metal-deposited DG compared to that on bare DG. The *m*-xylene adsorption strength is in the order of Pt₄-DG (-2.59 eV) > Pd₄-DG (-1.78 eV) > Au₄-DG (-1.48 eV) > Ag₄-DG (-1.22 eV). The average energy of electronic *d*-states, the *d*-band center (ϵ_d), is one of electronic charge properties used as a reactivity descriptor for metal catalysts.³⁶⁻³⁹ The shift of the *d*-band center upward from the fermi-level, the higher reactivity of the metal. For instance, the stronger oxygen chemisorption on Pt nanoclusters increases with the closer ϵ_d is to fermi level energy (E_F).⁴⁰ In this work, we found that *m*-xylene adsorption strength increases gradually with the upshift of ϵ_d toward E_F , which relates to the increasing of the substrate's

reactivity. **Figure 3b** shows the correlation between E_{ad} and ϵ_d values of the metal-deposited DG substrates.

The structures of *m*-xylene adsorption on substrates are visualized in **Figure 4**. Bond lengths and selected atomic distances are given in **Table 2**. The geometries of the adsorbate-substrate complexes are determined in this part. In *m*-xylene/Pt₄-DG, *m*-xylene is strongly bound to the Pt₄-DG with E_{ad} of -2.59 eV. Notably, Pt₄ is transformed to the distorted planar structure when it interacts to *m*-xylene, see **Figure 4a**. The Pt² atom has the interaction with C¹ and C⁶ atoms of *m*-xylene, while the Pt⁴ atom has contacts with C⁴ and C⁵ atoms of *m*-xylene (see **Table 2**). The average values of those Pt-C' lengths is about 2.15 Å. The distortion of the *m*-xylene structure can be observed when it is adsorbed on the metal-deposited DG. Compared to *m*-xylene in gas phase, the largest elongated bond is found between C⁵ and C⁶ atoms (~5.2%), while shortening length is observed at C²-C³ bond (~1.7%), in *m*-xylene/Pt₄-DG.

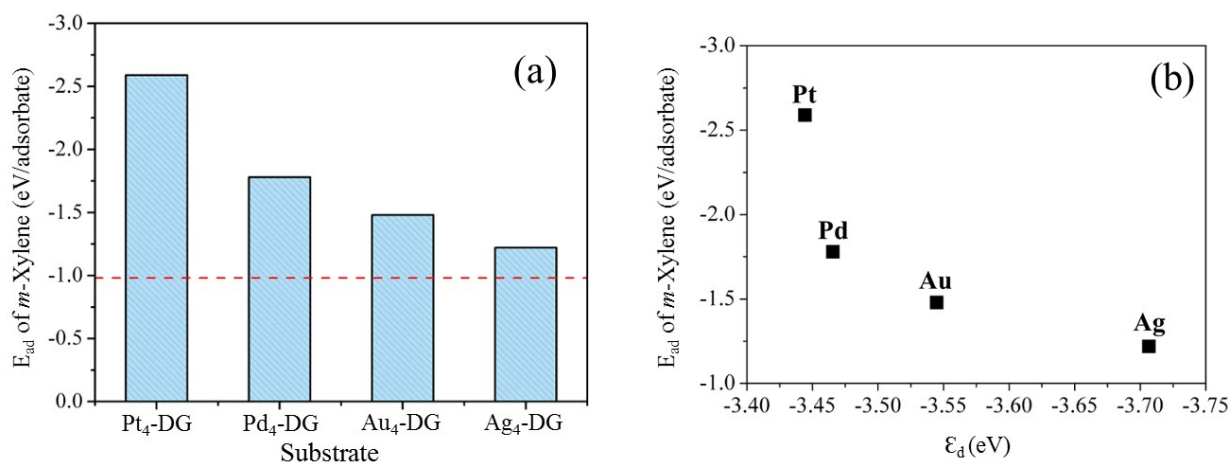


Figure 3. (a) Calculated E_{ad} of *m*-xylene on metal-deposited DG. Red dash line represents E_{ad} of *m*-xylene on PG, and (b) relationship between the E_{ad} values and the *d*-band center (ϵ_d) of the metal clusters on DG.

Table 2. Bond lengths (d) between i and j atoms in Å of the most stable structures of m -xylene adsorption on metal-deposited-DG calculated by PAWPBE with vdW (TS+SCS) method

Interacting components	Bond length, d (Å)			
	m -xylene/Pt ₄ -DG	m -xylene/Pd ₄ -DG	m -xylene/Au ₄ -DG	m -xylene/Ag ₄ -DG
Metal cluster ($M^i - M^j$)	Pt ¹ -Pt ² = 4.855	Pd ¹ -Pd ² = 3.234	Au ¹ -Au ⁴ = 2.534	Ag ¹ -Ag ³ = 2.707
	Pt ¹ -Pt ³ = 2.583	Pd ¹ -Pd ³ = 2.674	Au ² -Au ³ = 2.624	Ag ¹ -Ag ⁴ = 2.683
	Pt ¹ -Pt ⁴ = 2.560	Pd ¹ -Pd ⁴ = 2.709	Au ² -Au ⁴ = 2.698	Ag ² -Ag ³ = 2.708
	Pt ² -Pt ³ = 2.731	Pd ² -Pd ³ = 2.699	Au ³ -Au ⁴ = 2.617	Ag ² -Ag ⁴ = 2.685
	Pt ² -Pt ⁴ = 3.189	Pd ² -Pd ⁴ = 2.782		Ag ³ -Ag ⁴ = 2.782
	Pt ³ -Pt ⁴ = 2.616	Pd ³ -Pd ⁴ = 2.660		
Metal—C of graphene ($M^i - C^j$)	Pt ³ -C ¹ = 1.962	Pd ³ -C ¹ = 1.926	Au ³ -C ¹ = 2.038	Ag ³ -C ¹ = 2.290
	Pt ³ -C ² = 1.960	Pd ³ -C ² = 1.948	Au ³ -C ² = 2.176	Ag ³ -C ² = 2.105
	Pt ³ -C ³ = 1.984	Pd ³ -C ³ = 1.942	Au ³ -C ³ = 2.039	Ag ³ -C ³ = 2.106
Metal—C' of m -xylene ($M^i - C'^j$)	Pt ² -C' ¹ = 2.147	Pd ¹ -C' ⁴ = 2.212	Au ¹ -C' ¹ = 2.943	Ag ⁴ -C' ³ = 2.933
	Pt ² -C' ⁶ = 2.171	Pd ² -C' ¹ = 2.406	Au ¹ -C' ² = 2.279	Ag ⁴ -C' ⁴ = 2.462
	Pt ⁴ -C' ⁴ = 2.158	Pd ² -C' ⁶ = 2.206	Au ¹ -C' ³ = 2.476	Ag ⁴ -C' ⁵ = 2.779
	Pt ⁴ -C' ⁵ = 2.139	Pd ⁴ -C' ⁵ = 2.083		

	$C^{i1}-C^{j2} = 1.449 (+3.4\%)$	$C^{i1}-C^{j2} = 1.419 (+1.3\%)$	$C^{i1}-C^{j2} = 1.428 (+1.9\%)$	$C^{i1}-C^{j2} = (+0.1\%)$
	$C^{i2}-C^{j3} = 1.377 (-1.7\%)$	$C^{i2}-C^{j3} = 1.396 (-0.3\%)$	$C^{i2}-C^{j3} = 1.427 (+1.9\%)$	$C^{i2}-C^{j3} = (0.0\%)$
	$C^{i3}-C^{j4} = 1.449 (+3.3\%)$	$C^{i3}-C^{j4} = 1.431 (+2.1\%)$	$C^{i3}-C^{j4} = 1.416 (+1.0\%)$	$C^{i3}-C^{j4} = (+1.0\%)$
<i>m</i> -Xylene	$C^{i4}-C^{j5} = 1.438 (+2.9\%)$	$C^{i4}-C^{j5} = 1.460 (+4.5\%)$	$C^{i4}-C^{j5} = 1.388 (-0.6\%)$	$C^{i4}-C^{j5} = (+0.8\%)$
$(C^i - C^j)$	$C^{i5}-C^{j6} = 1.469 (+5.2\%)$	$C^{i5}-C^{j6} = 1.454 (+4.1\%)$	$C^{i5}-C^{j6} = 1.406 (+0.7\%)$	$C^{i5}-C^{j6} = (+0.1\%)$
	$C^{i1}-C^{j6} = 1.444 (+3.0\%)$	$C^{i1}-C^{j6} = 1.426 (+1.7\%)$	$C^{i1}-C^{j6} = 1.392 (-0.7\%)$	$C^{i1}-C^{j6} = (+0.2\%)$
	$C^{i1}-C^{j8} = 1.512 (+0.3\%)$	$C^{i1}-C^{j8} = 1.510 (+0.2\%)$	$C^{i1}-C^{j8} = 1.501 (-0.4\%)$	$C^{i1}-C^{j8} = (-0.3\%)$
	$C^{i3}-C^{j7} = 1.499 (-0.5\%)$	$C^{i3}-C^{j7} = 1.506 (-0.1\%)$	$C^{i3}-C^{j7} = 1.506 (-0.1\%)$	$C^{i3}-C^{j7} = (-0.3\%)$

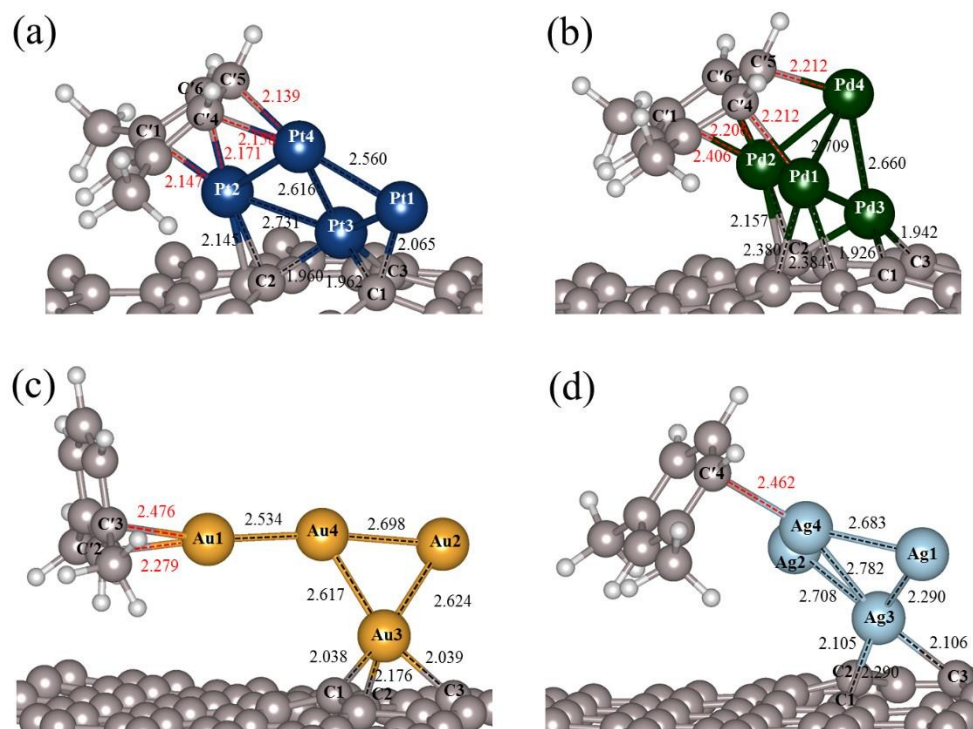


Figure 4. The *m*-xylene adsorption on metal cluster-deposited DG (a) *m*-xylene/Pt₄-DG, (b) *m*-xylene/Pd₄-DG, (c) *m*-xylene/Au₄-DG and (d) *m*-xylene/Ag₄-DG. Blue, green, yellow, light blue, grey and white balls represent Pt, Pd, Au, Ag, C and H atoms, respectively.

The *m*-xylene/Pd₄-DG structure is shown in **Figure 4b**. The Pd₄ retains the distorted tetrahedral geometry after interacted with *m*-xylene. Considering the *m*-xylene structure, the C'⁴-C'⁵ length is increased about 4.2% when it is adsorbed on the Pd₄-DG substrate. Three Pd atoms (*i.e.* Pd¹, Pd² and Pd⁴) interact with C' atoms of *m*-xylene with distances in range of 2.1 to 2.4 Å.

Tilting of the C-H bonds indicated the formation of C-metal bonds when *m*-xylene is chemically adsorbed on Pt₄-DG and Pd₄-DG. In the *m*-xylene/Pt₄-DG structure, H atoms attached to C'¹, C'⁴, C'⁵ and C'⁶ atoms are tilted in range of 15° to 35° from the molecular plane. Similarly,

H atoms attached to C⁴, C⁵ and C⁶ atoms of the *m*-xylene/Pd₄-DG structure are tilted in range of 15° to 30° from the molecular plane. In the literature, this tilting can be found when aromatic compounds are chemically adsorbed on metal surfaces and metal clusters.^{20, 41-43} Clearly, the adsorption of *m*-xylene on Pt₄- and Pd₄-DG substrates occurs via the chemisorption process, indicated by metal- C' bond lengths and tilting of H atoms of *m*-xylene.

In the other two substrates, the maximum elongation of bond lengths of *m*-xylene on Au₄-DG (see **Figure 4c**) and Ag₄-DG (see **Figure 4d**) are ~1.9% and ~1.0%, respectively. C'-H bonds of *m*-xylene are slightly bent (less than 7°) in these two systems. Obviously, *m*-xylene on Au₄- and Ag₄-DG substrates are less significantly distorted than those on Pt₄- and Pd₄-DG substrates. The attraction between *m*-xylene and Au₄- and Ag₄-DG substrates dominates by the physisorption. Evidently, the variation of the *m*-xylene structure corresponds to the tendency of the calculated E_{ad} values. The *m*-xylene adsorption on small cluster-deposited graphene in this work shows the similar behavior as the benzene adsorption on pure metal surfaces determined by Liu *et al.*⁴³ Liu *et al.* asserted that benzene is adsorbed strongly by the chemisorption on Pt, Pd, Ir and Rh surfaces, but it has weak interaction to Ag and Au surfaces through physisorption

3.2.2 Electronic properties

In the last section, the electronic charge properties of the bare substrates and the adsorbate-substrate complexes are determined in order to understand insight to the nature of their interactions. It is to be noted that Pt and Pd atoms have 10-valence electrons, while Au and Ag atoms have 11-valence electrons. Therefore, the quantitative charge properties can not be compared explicitly between different series of metals. First, the projected density of states (PDOSs) are analyzed in this section. PDOSs of metals and carbon atoms are compared in **Figure 5a-d**. The total density

of states (DOSs) were projected on to *s*- and *p*-orbitals of C atoms, *s*- and *d*-orbitals of metal atoms and *s*-orbital of H atoms. The Fermi energy (E_F) is shifted to 0.0 eV. In **Figure 5**, PDOSs of the isolated metal cluster and bare DG are plotted in the panel I. PDOSs of each bare substrate is plotted in the panel II. For the substrate-adsorbate structure, PDOSs of the substrate and *m*-xylene are shown in the panel III and the panel IV, respectively.

In bare DG (see the panel I), PDOS peak of C atoms arisen at E_F identifies the dangling bonds at the defect site. This characteristic peak at E_F does not exist in PDOS of PG as shown in **Figure S5a**. Broadening of *d*-DOS in all four metal clusters significantly occurs when they are attached to DG (see the panel II of **Figure 5**). Disappearing of the peak of C atoms at E_F and broadening of *d*-DOS of the metal indicates bond formation between metal and C atoms at the defect site. Also, the PDOSs of the four substrates are changed upon the *m*-xylene adsorption. In *d*-band metals, the *s*-band coupling is not dominant, thus *d*-DOS hybridizes with DOS of an adsorbate are designated interactions between *d*-band metals and *m*-xylene molecules. In the isolated *m*-xylene molecule (see **Figure S5c**), the overlapping of orbitals of C' and H atoms is expressed the C'-H bonds. The bonding and anti-bonding states are designated at below and above E_F , respectively. Those states are significantly redistributed when *m*-xylene is bound on the substrates as illustrated in the panel IV of **Figure 5**.

The PDOSs of the isolated Pt₄ and bare DG are shown in the panel I of **Figure 5a**. In the isolated Pt₄ cluster, the *s-d* hybridization is indicated by overlapping of the *s*- and *d*-peaks. PDOSs of Pt₄-DG is presented in the panel II of **Figure 5a**. The *d*-DOS peak of the Pt₄ is broadening when it binds with DG. The panel III and IV of **Figure 5a** are PDOSs of Pt₄-DG and *m*-xylene in the *m*-xylene/Pt₄-DG structure, respectively. Broad distribution of PDOSs of the Pt₄ can be identified after binding with DG and *m*-xylene. **Figure 5a**-panel III presents PDOSs of *m*-xylene/Pt₄-DG.

The d - p hybridization of Pt³ and C atoms at the defect site has the major contribution in d -DOS at the energy lower than -4.5 eV. Most d -states of other Pt atoms are located in range of -4.5 eV to E_F . When PDOSs of m -xylene are considered, the s - p hybridization of the C'-H bonds occurs at the energy lower than ~ 4 eV. Moreover, the overlapping of d -DOS of Pt₄ (in the panel III) and p -DOS of C' (in the panel IV) indicates the interaction between Pt₄ and m -xylene as mentioned in the previous part. The strong overlapping aspects of PDOSs at -4.5 and -3.5 eV relate to the Pt-C' bonds illustrated in **Figure 4a**. For anti-bonding states, the predominant d -DOS peak (positioned at ~ 1 eV in the panel III) of Pt₄ of Pt₄-DG is diminished when Pt₄-DG adsorbs m -xylene. Otherwise, that band is overlapped with p -DOS of C' atoms of m -xylene in range of 1 to 3 eV, which indicates the interaction between them.

For the m -xylene/Pd₄-DG system, the comparison of PDOS of the bare substrate till the m -xylene adsorption are expressed in **Figure 5b**. The expansion of d -DOS of Pd₄ also appears when Pd₄ is deposited on DG. The s - p hybridization of PDOS of H and C' atoms of m -xylene exists at the energy lower than -4.5 eV as shown in the panel IV of **Figure 5b**. Similar to the m -xylene/Pt₄-DG system, the characteristic peak around -3.5 eV corresponds to the Pd-C' bonding states. Considering the anti-bonding states, d -DOS of Pd atoms (in the panel III) and p -DOS of C' atoms (in the panel IV) are overlapped at the energy above ~ 0.5 eV.

In the $4d$ metal systems, the expansion of PDOSs of Au₄ and Ag₄ clusters can be observed upon depositing on DG. In the m -xylene/Au₄-DG system, the overlapping of PDOSs of Au and C' atoms presents at the energy lower than -1.25 eV as illustrated in **Figure 5c**. The hybridization of anti-bonding states of the free substrate and the adsorbate are weaker than that in m -xylene/Pt₄-DG and m -xylene/Pd₄-DG. In the m -xylene/Ag₄-DG system, the hybridization of d -DOS of Ag atoms p -DOS of C' atoms appears at the energy lower than -1.50 eV, where the weak hybridization

is observed ~ 1 eV above E_F . The d -DOS peak of Ag_4 -DG is slightly changed upon m -xylene adsorption. The hybridization between bands of m -xylene and those substrates is one of properties that describes the interaction between them. The m -xylene/ Pt_4 -DG and m -xylene/ Pd_4 -DG complexes express the stronger hybridization feature compared to other two systems. Hence, this provides support to the E_{ad} calculations discussed in the earlier part.

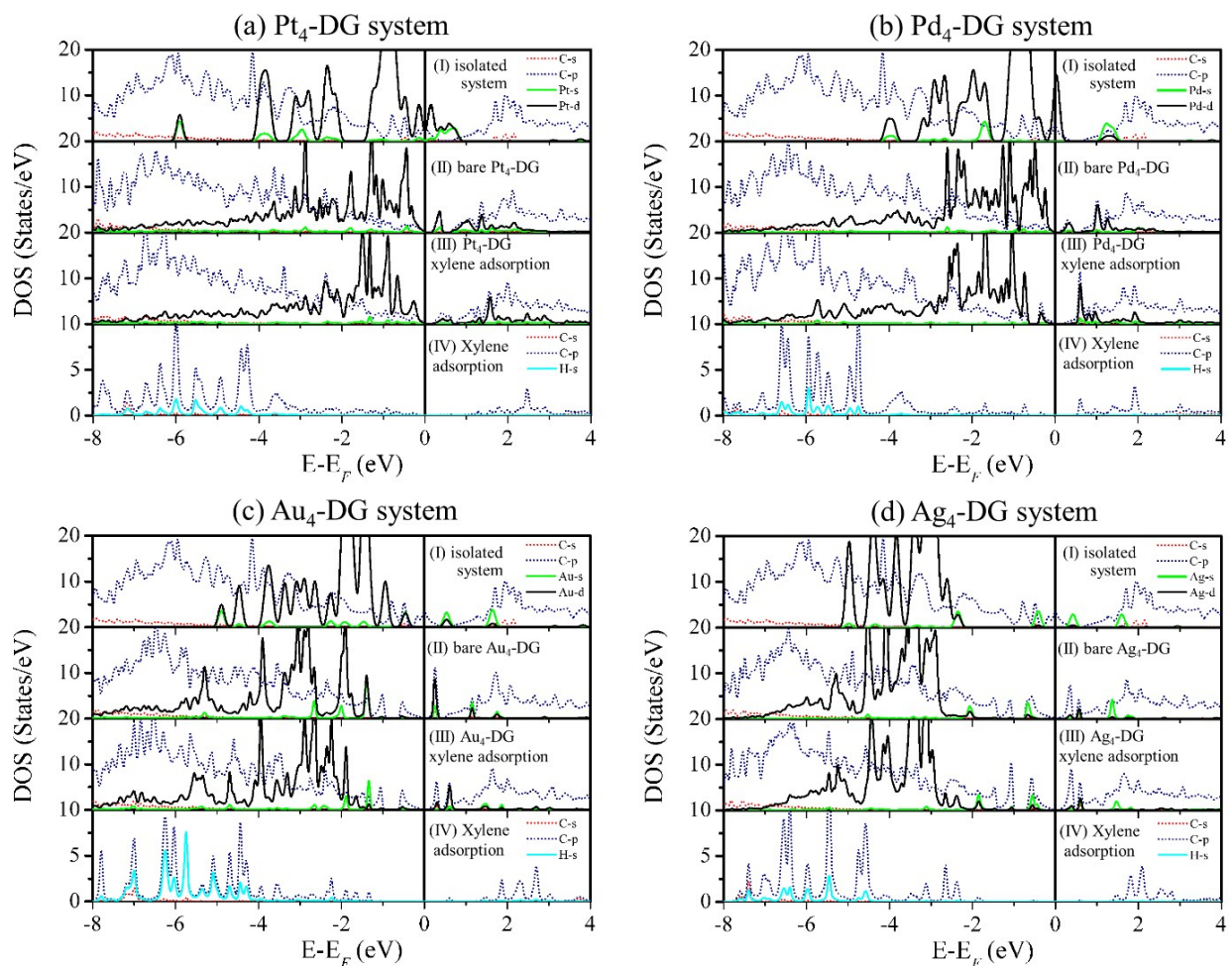


Figure 5. Comparison projected density of states (PDOS) of metals and carbon of (a) the Pt_4 -DG system, (b) the Pd_4 -DG system, (c) the Au_4 -DG system and (d) the Ag_4 -DG system. In each system, the panel I presents PDOS of the isolated metal cluster and the bare DG. The panel II presents PDOS of the metal-deposited DG before adsorbing m -xylene. The panel III presents PDOS of the

metal-deposited defective graphene bound to *m*-xylene. The panel IV presents PDOS of *m*-xylene on the substrate.

The second electronic charge property is the charge difference analysis. Comparison of charge density difference in the metal-deposited DG are revealed in **Figure 6(a)-(d)**. Charge accumulation and charge depletion are expressed by blue and red surfaces, respectively. Charge accumulation is mainly observed in the bonding area between metal atom and the three nearest C atoms at the defective site. Intensity of charge difference is as the following order: Pt₄-DG > Pd₄-DG > Au₄-DG > Ag₄-DG, at the same isovalue of $\pm 5 \times 10^{-3} e/\text{\AA}^3$. This trend relates to the order of calculated E_{ad} values of metal clusters on DG reported in the previous section. For the *m*-xylene adsorbed-substrates, charge difference are visualized by the isovalue of $\pm 1.5 \times 10^{-3}$ as shown in **Figure 6e-6h**. Electrons donation from metal clusters to DG are clearly spotted in the metal-deposited DG.

During *m*-xylene adsorption, the increment of electrons can be observed in the graphene sheet and *m*-xylene, whereas electrons in metal clusters are reduced. Charge depletion of π -electron on *m*-xylene rings can be observed in all cases. Details of charge distribution are examined in the later part.

Table 3. Bader charge results (where plus and minus signs denote the increment and reduction of electrons, respectively)

System	Change of Bader charges (electron)				
	metal cluster-DG		<i>m</i> -xylene/metal cluster-DG		
	Metal cluster	DG	Metal cluster	DG	<i>m</i> -xylene
Pt ₄ -DG	Total (-0.209)	Total (+0.209)	Total (-1.381)	Total (+0.833)	Total (+0.548)
	Pt ¹ (-0.002)	C ¹ (+0.169)	Pt ¹ (-0.047)	C ¹ (+0.448)	C ¹ (+0.168)
	Pt ² (-0.040)	C ² (+0.080)	Pt ² (-0.400)	C ² (+0.397)	C ⁴ (-0.142)
	Pt ³ (-0.412)	C ³ (+0.068)	Pt ³ (-0.873)	C ³ (+0.216)	C ⁵ (-0.332)
	Pt ⁴ (+0.244)		Pt ⁴ (-0.060)		C ⁶ (-0.090)
Pd ₄ -DG	Total (-0.316)	Total (+0.316)	Total (-1.081)	Total (+0.636)	Total (+0.446)
	Pd ¹ (-0.082)	C ¹ (-0.062)	Pd ¹ (-0.281)	C ¹ (+0.102)	C ¹ (+0.106)
	Pd ² (-0.088)	C ² (+0.114)	Pd ² (-0.455)	C ² (+0.290)	C ⁴ (-0.206)
	Pd ³ (-0.360)	C ³ (+0.129)	Pd ³ (-0.258)	C ³ (+0.152)	C ⁵ (-0.007)
	Pd ⁴ (+0.216)		Pd ⁴ (-0.087)		C ⁶ (-0.091)
Au ₄ -DG	Total (-0.067)	Total (+0.067)	Total (-0.374)	Total (+0.281)	Total (+0.093)
	Au ¹ (+0.168)	C ¹ (+0.090)	Au ¹ (-0.147)	C ¹ (+0.162)	C ¹ (-0.021)
	Au ² (+0.142)	C ² (+0.325)	Au ² (+0.047)	C ² (-0.021)	C ² (-0.154)
	Au ³ (-0.366)	C ³ (+0.032)	Au ³ (-0.444)	C ³ (+0.109)	C ³ (-0.083)
	Au ⁴ (-0.011)		Au ⁴ (+0.170)		
Ag ₄ -DG	Total (-0.454)	Total (+0.455)	Total (-0.549)	Total (+0.367)	Total (+0.182)
	Ag ¹ (-0.024)	C ¹ (+0.090)	Ag ¹ (+0.064)	C ¹ (-0.128)	C ³ (-0.204)
	Ag ² (-0.026)	C ² (+0.032)	Ag ² (-0.063)	C ² (+0.005)	C ⁴ (-0.035)
	Ag ³ (-0.365)	C ³ (+0.325)	Ag ³ (-0.334)	C ³ (+0.010)	C ⁵ (+0.042)
	Ag ⁴ (-0.040)		Ag ⁴ (-0.216)		

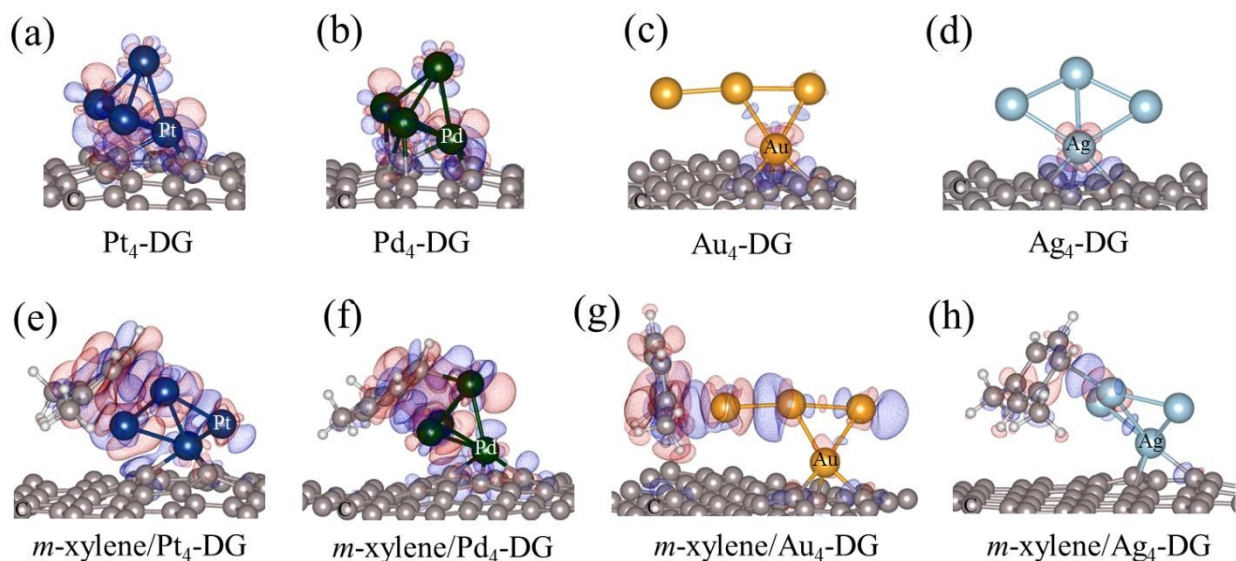


Figure 6. Charge difference in the bare substrates (a) Pt₄-DG, (b) Pd₄-DG, (c) Au₄-DG and (d) Ag₄-DG are presented with isovalue of $\pm 5 \times 10^{-3} e/\text{\AA}^3$. Charge difference in the *m*-xylene/metal cluster-DG (e) *m*-xylene/Pt₄-DG, (f) *m*-xylene/Pd₄-DG, (g) *m*-xylene/Au₄-DG and (h) *m*-xylene/Ag₄-DG are presented with isovalue of $\pm 1.5 \times 10^{-3} e/\text{\AA}^3$. Blue and red colors represent the charge accumulation and depletion regions, respectively.

In addition, a bader analysis^{44,45} was performed in this part. Charge analysis of selected atoms was reported in **Table 3**. Atomic indexes are assigned in **Figure 4**. The number of valence electrons of a neutral atom is used as a reference for calculating change of Bader charges. Plus and minus signs denote charge increment and charge reduction, respectively. In all bare metal cluster-DGs, metal clusters donate their electrons to DG component. This aspect corresponds to previous work⁴⁶. During *m*-xylene adsorption, increment of electrons can be observed in DG and *m*-xylene, while electrons of metal clusters are reduced. As mentioned earlier, charge quantities can not be compared explicitly between different series of metals. In Pt₄-DG and Pd₄-DG substrates, Pt³ and

Pd³ atoms are attached at defect sites of DG. Even if the change of total charges in bare Pd₄-DG substrate is higher than that in bare Pt₄-DG, the dissipated charges of Pt³ (~0.41 e) is greater than that in Pd³ atom. (~0.36 e). When Pt₄-DG and Pd₄-DG substrates adsorb *m*-xylene, *m*-xylene gains more electrons from Pt₄-DG than that from Pd₄-DG. Therefore, charge transfer would assist the chemisorption between *m*-xylene and these two substrates. In bare Au₄-DG and Ag₄-DG substrates, the anchored atoms (Au³ and Ag³) located at the vacancy site lose their electrons to DG about 0.37 e. Charge distribution of individual atoms are different due to the different shapes of Au₄ and Ag₄ clusters. In the *m*-xylene/Au₄-DG system, the Au¹ atom interacts with *m*-xylene molecule, then its charges is reduced. Similarly, charge reduction can be observed at the Ag⁴ atom interacted with C' of *m*-xylene in *m*-xylene/Ag₄-DG system. In contrast with Pt₄-DG and Pd₄-DG, change of Bader charges are not clearly explained the order of binding strength between *m*-xylene and the Au₄-DG or the Ag₄-DG due to the physisorption.

The electronic charge properties supported the results from the structural and energetic properties. Large amount of charge transfer from the substrate to the adsorbate and the hybridization of PDOSs describe the strong interaction between the adsorbate and the substrate in *m*-xylene/Pt₄-DG and *m*-xylene/Pd₄-DG systems, which clearly indentify chemisorption. In *m*-xylene/Au₄-DG and *m*-xylene/Ag₄-DG systems, on the other hand, the physisorption is identified. The weak interaction between the adsorbate and the substrate, which is mostly accounted by vdW interaction, was explained by small amount of electron transfer and weak hybridization of the PDOS..

4. Conclusions

From our calculations Pt₄, Pd₄, Au₄ and Ag₄ clusters have excellent interactions with DG while their interactions with PG are comparatively less. The high binding strength originates from the hybridizations of *p*-orbitals of carbon atoms at the DG's vacancy and *d*-orbitals of the metal atoms bonding with the carbon atoms, which describe the formation of the new strong interfacial bonds. The explicit charges transferred from the cluster to the graphene support are observed and show strong correlation with the binding energy, indicating that the 5*d* metal clusters (Pt₄ and Pd₄) are attached to the graphene significantly stronger than the 4*d* metal clusters (Au₄ and Ag₄). Then, the metal-DGs were selected as sorbents for investigating the *m*-xylene adsorption. The *m*-xylene adsorption energy is found in the order of Pt₄-DG (-2.59 eV) > Pd₄-DG (-1.78 eV) > Au₄-DG (-1.48 eV) > Ag₄-DG (-1.22 eV). This energy trend is closely related to the *d*-band center (ϵ_d) of the deposited metals of the pre-adsorbed sorbents in which the ϵ_d shifts upward to the fermi level, the higher reactivity of the sorbents to *m*-xylene and higher adsorption strength are achieved. The two classes of *m*-xylene interaction with the sorbents, chemisorption and physisorption, are derived. The calculated adsorption energy, structural distortion of *m*-xylene and electronic properties indicate that the interactions of *m*-xylene on Pt₄- and Pd₄-DG sorbents are chemisorption, while those on Au₄-and Ag₄-DG sorbents are physisorption. The present results demonstrate that the reactivity of carbon materials can be tuned by modulating of deposited metals. These information will be a guideline for modifying carbon-based materials for specific purposes, such as VOCs abatement processes by adsorption or catalytic oxidation.

5. Acknowledgement

Calculations were carried out on the computer facilities of National e-Science Infrastructure Consortium, Thailand, and Texas A&M University, USA.

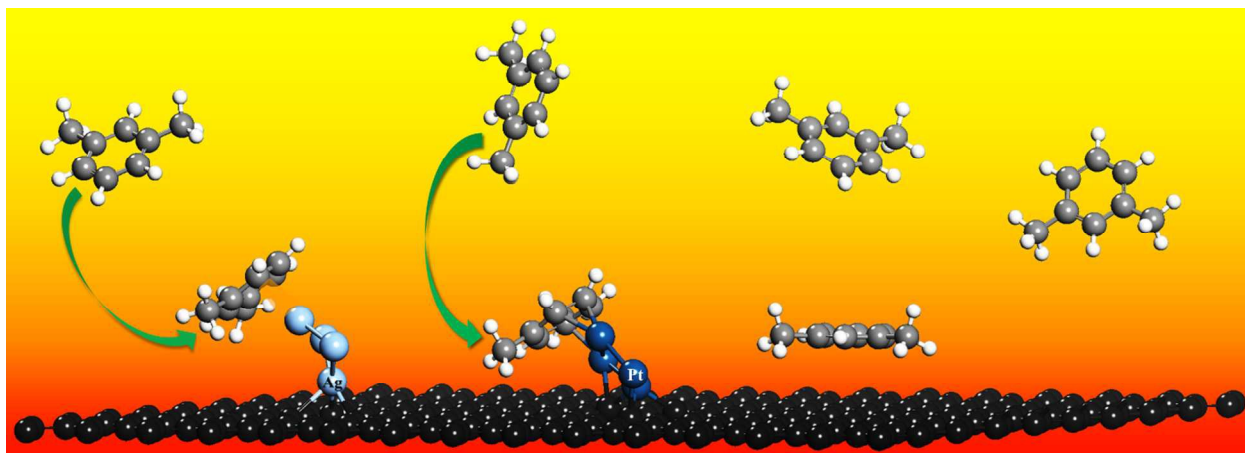
Supporting Information: The optimized geometries of metal clusters on PG and DG as well as their electronic properties are provided.

References

1. B. J. Finlayson-Pitts and J. N. Pitts, *Science*, 1997, **276**, 1045-1051.
2. M. Hakim, Y. Y. Broza, O. Barash, N. Peled, M. Phillips, A. Amann and H. Haick, *Chem. Rev.*, 2012, **112**, 5949-5966.
3. R. Atkinson, *Atmos. Environ.*, 2000, **34**, 2063-2101.
4. M. Słomińska, S. Król and J. Namieśnik, *Crit. Rev. Env. Sci. Technol.*, 2012, **43**, 1417-1445.
5. B. R. Kim, *Environ. Eng. Res.*, 2011, **16**, 1-9.
6. F. I. Khan and A. Kr. Ghoshal, *J. Loss Prevent. Proc.*, 2000, **13**, 527-545.
7. J. Zhao and X. Yang, *Build. Environ.*, 2003, **38**, 645-654.
8. S. Wang, H. M. Ang and M. O. Tade, *Environ. Int.*, 2007, **33**, 694-705.
9. M. H. El-Naas, J. A. Acio and A. E. El Telib, *J. Environ. Chem. Eng.*, 2014, **2**, 1104-1122.
10. N. A. Khan, Z. Hasan and S. H. Jung, *J. Hazard. Mater.*, 2013, **244–245**, 444-456.
11. A. D. Luz, S. M. d. A. Guelli Ulson de Souza, C. da Luz, R. V. d. P. Rezende and A. A. Ulson de Souza, *Ind. Eng. Chem. Res.*, 2013, **52**, 7896-7911.
12. M. J. Lashaki, M. Fayaz, H. Wang, Z. Hashisho, J. H. Philips, J. E. Anderson and M. Nichols, *Environ. Sci. Technol.*, 2012, **46**, 4083-4090.
13. C.-Y. Lu and M.-Y. Wey, *Fuel Process. Technol.*, 2007, **88**, 557-567.
14. J. C.-S. Wu, Z.-A. Lin, F.-M. Tsai and J.-W. Pan, *Catal. Today*, 2000, **63**, 419-426.
15. W. G. Shim and S. C. Kim, *App. Surf. Sci.*, 2010, **256**, 5566-5571.

16. K.-J. Kim, C.-S. Kang, Y.-J. You, M.-C. Chung, M.-W. Woo, W.-J. Jeong, N.-C. Park and H.-G. Ahn, *Catal. Today*, 2006, **111**, 223-228.
17. M. C. Tsai and E. L. Muetterties, *J. Am. Chem. Soc.*, 1982, **104**, 2534-2539.
18. H. Yildirim, T. Greber and A. Kara, *J. Phys. Chem. C*, 2013, **117**, 20572-20583.
19. P. D. Cernota, H. A. Yoon, M. Salmeron and G. A. Somorjai, *Surf. Sci.*, 1998, **415**, 351-362.
20. M. T. d. M. Cruz, J. W. d. M. Carneiro, D. A. G. Aranda and M. Bühl, *J. Phys. Chem. C*, 2007, **111**, 11068-11076.
21. P. De Souza, D. Aranda, D. M. Carneiro, D. S. De Oliveira, O. Antunes and F. Passos, *Int. J. Quantum Chem.*, 2003, **92**, 400-411.
22. V. Gaur, A. Sharma and N. Verma, *Carbon*, 2005, **43**, 3041-3053.
23. H. Shaoyong, Z. Changbin and H. Hong, *J. Environ. Sci.*, 2009, **21**, 985-990.
24. J. Paier, R. Hirschl, M. Marsman and G. Kresse, *J. Chem. Phys.*, 2005, **122**, 234102.
25. G. Kresse and D. Joubert, *Phys. Rev. B*, 1999, **59**, 1758-1775.
26. G. Kresse and J. Hafner, *Phys. Rev. B*, 1993, **47**, 558-561.
27. G. Kresse and J. Furthmüller, *Phys. Rev. B*, 1996, **54**, 11169-11186.
28. T. Bučko, S. Lebègue, J. Hafner and J. G. Ángyán, *Phys. Rev. B*, 2013, **87**, 064110.
29. L. Xiao and L. Wang, *J. Phys. Chem. A*, 2004, **108**, 8605-8614.
30. X. Lin, N. J. Ramer, A. M. Rappe, K. C. Hass, W. F. Schneider and B. L. Trout, *J. Phys. Chem. B*, 2001, **105**, 7739-7747.
31. A. M. Ferrari, C. Xiao, K. M. Neyman, G. Pacchioni and N. Rosch, *Phys. Chem. Chem. Phys.*, 1999, **1**, 4655-4661.
32. J. Wang, G. Wang and J. Zhao, *Phys. Rev. B*, 2002, **66**, 035418.
33. B. Chan and W.-L. Yim, *J. Chem. Theory Comput.*, 2013, **9**, 1964-1970.
34. C. Majumder and S. K. Kulshreshtha, *Phys. Rev. B*, 2006, **73**, 155427.
35. A. Singh, C. Majumder and P. Sen, *J. Chem. Phys.*, 2014, **140**, 164705-164701-164705-164708.
36. B. Hammer and J. K. Nørskov, *Nature*, 1995, **376**, 238-240.
37. H. Xin, A. Vojvodic, J. Voss, J. K. Nørskov and F. Abild-Pedersen, *Phys. Rev. B*, 2014, **89**, 115114.
38. B. Hammer and J. K. Nørskov, *Surf. Sci.*, 1995, **343**, 211-220.

39. B. Hammer and J. K. Nørskov, in *Advances in Catalysis*, ed. H. K. Bruce C. Gates, Academic Press, 2000, vol. Volume 45, pp. 71-129.
40. E. Toyoda, R. Jinnouchi, T. Hatanaka, Y. Morimoto, K. Mitsuhashi, A. Visikovskiy and Y. Kido, *J. Phys. Chem. C*, 2011, **115**, 21236-21240.
41. C. Morin, D. Simon and P. Sautet, *J. Phys. Chem. B*, 2004, **108**, 12084-12091.
42. S. J. Jenkins, *Proc. R. Soc. A*, 2009, **465**, 2949-2976.
43. W. Liu, J. Carrasco, B. Santra, A. Michaelides, M. Scheffler and A. Tkatchenko, *Phys. Rev. B*, 2012, **86**, 245405.
44. W. Tang, E. Sanville and G. Henkelman, *J. Phys.: Condens. Matter.*, 2009, **21**, 084204.
45. G. Henkelman, A. Arnaldsson and H. Jónsson, *Comput. Mater. Sci.*, 2006, **36**, 354-360.
46. I. Fampiou and A. Ramasubramaniam, *J. Phys. Chem. C*, 2012, **116**, 6543-6555.



m-Xylene weakly adsorbs on graphene and silver cluster doped graphene, but it has excellent interaction with platinum cluster doped graphene.